nanomaterials

MDPI

Communication

Design of Superhydrophobic $CoFe_2O_4$ Solar Seawater Desalination Device and Its Application in Organic Solvent Removal

Xiangcai Ge [1], Zhijun Zhou [1], Zheng Tan [1], Shoufei Wang [1], Xingchuan Zhao [1,*], Guina Ren [2], Bo Ge [1,*] and Wei Li [1]

[1] School of Materials Science and Engineering, Liaocheng University, Liaocheng 252059, China; gexiangcai@lcu.edu.cn (X.G.); 2020205938@stu.lcu.edu.cn (Z.Z.); 2019205643@stu.lcu.edu.cn (Z.T.); 2018206124@stu.lcu.edu.cn (S.W.); liwei@lcu.edu.cn (W.L.)

[2] School of Environmental and Material Engineering, Yantai University, Yantai 264405, China; guina.ren@ytu.edu.cn

* Correspondence: zhaoxingchuan@lcu.edu.cn (X.Z.); gebo@lcu.edu.cn (B.G.)

Abstract: Environmental pollution and clean water production are challenges to the development of human society. In this paper, devices consisting of a superhydrophobic Ni-$CoFe_2O_4$ foam layer (floating layer), a hydrophilic channel and a superhydrophilic Ni-$CoFe_2O_4$ foam layer (photothermal conversion layer) were designed. The light energy was converted into heat on the photothermal layer, for which the hydrophilic channel provided a small amount of water. The superhydrophobic layer ensured the floating and selective adsorption of organic solvents on the water surface, whose contact angle reached 157°, and the steam production rate reached 1.68 $kg \cdot m^{-2} \cdot h^{-1}$. Finally, the LSV curve demonstrated that the Ni-$CoFe_2O_4$ foam prepared had a minimum starting potential, achieving the multifunctionality of the Ni foam.

Keywords: superhydrophobic; oil–water separation; clean water production

Citation: Ge, X.; Zhou, Z.; Tan, Z.; Wang, S.; Zhao, X.; Ren, G.; Ge, B.; Li, W. Design of Superhydrophobic $CoFe_2O_4$ Solar Seawater Desalination Device and Its Application in Organic Solvent Removal. *Nanomaterials* **2022**, *12*, 1531. https://doi.org10.3390/nano12091531

Academic Editor: Ana C. Perdigón

Received: 29 March 2022
Accepted: 28 April 2022
Published: 2 May 2022

1. Introduction

Environmental and drinking water safety is a global challenge that hinders social development [1,2]. Statistics show that water consumption will grow by >55% by 2050 with the increase in GDP [3]. Desalination is an important way to solve water shortage. At present, desalination methods mainly include thermal and membrane separation methods (RO), accounting for more than 90% of the market. Traditional RO methods have an energy consumption of 3.5 kWh_{elec}/m^3 [4]. The enthalpy of evaporation (ΔH) needs to be overcome for thermal methods, and the separation energy (ΔG) needs to be overcome for filtration methods. ΔH is two orders of magnitude higher than ΔG [5]. Compared with seawater desalination methods that consume fossil fuels, only solar energy is used in solar desalination to produce clean water, which has attracted wide attention from researchers [6,7]. Through the modification of polydopamine and $Ti_3C_2T_x$ Mxenes, Chen et al. [8] used balsa wood as a raw material to obtain an evaporator, which had a high steam production speed of 2.08 $kg \cdot m^{-2} \cdot h^{-1}$. Lin et al. [9] loaded poly(N-phenylglycine) and MoS_2 on a polyvinylidene fluoride (PVDF) film to form a photothermal layer. A steam production rate of 1.7 $kg \cdot m^{-2} \cdot h^{-1}$ was obtained for the photothermal device, assisted by hydrophilic channels and polystyrene foam. When photothermal technology is applied to sewage discharged from chemical plants, the problem of floating organic solvent pollutants needs to be solved. Superhydrophobic–superoleophilic materials have attracted research interests due to their ability to selectively adsorb organic solvents [10,11]. Liu et al. [12] prepared superhydrophobic silica floating on the oil–water interface, which could selectively adsorb the oil phase to achieve the purpose of oil–water separation. However, superhydrophobic silica is difficult to recover from the powder state.

In order to realize floating oil removal and clean water production, a multifunctional solar evaporator was designed, which is composed of a superhydrophobic floating layer, a filter paper layer and a $CoFe_2O_4$ photothermal layer. The superhydrophobic layer has two functions: one is to selectively adsorb floating oil and the other is to support the floating of the device. Through the synergy of the three layers, a solar evaporation rate of 1.68 $kg \cdot m^{-2} \cdot h^{-1}$ was obtained by the device, providing a new solution for the application of solar evaporators in sewage treatment.

2. Experimental Section

2.1. Material

HCl (AR, 36–38 wt %), acetone (AR, 99.5%) and ethanol (AR, 99.7%) were supplied by Yantai Far East Fine Chemical Co., Ltd. $FeCl_2$ $4H_2O$ (AR, 99.7%) was purchased from Tianjin Fuchen Chemical Reagents Factory. $Co(NO_3)_2$ $6H_2O$ (AR, 99%), NHF (AR, 98%), $CO(NH_2)_2$ and Trichloro(1H, 1H, 2H, 2H-tridecafluoro-n-octyl)silane (AR, 97%) were provided by Aladdin Chemical Reagent Co., Ltd. Nickel foam was purchased from a local store.

2.2. Preparation of Solar Evaporator

The nickel foam was cut to the size of 3.5 cm × 3.5 cm and sonicated in 3 mol/L HCl, deionized water, acetone and ethanol for 20 min each. Amounts of 0.1592 g of $FeCl_2 \bullet 4H_2O$, 0.4656 g of $Co(NO_3)_2 \bullet 6H_2O$, 0.0592 g of NH_4F and 0.2402g of urea were dissolved in 65 mL of deionized water and transferred to a 100 mL stainless-steel autoclave. Nickel foam was added, reacting at 140 °C for 8 h. After cooling, the samples were dried at 140 °C for 0.5 h and then sintered at 400 °C for 3 h (heating speed was 2 °C/min). The resulting superhydrophilic Ni-$CoFe_2O_4$ foam was named the photothermal conversion layer. The floating layer was prepared as follows: the superhydrophilic Ni/$CoFe_2O_4$ foam was added to 30 mL of silane ethanol solution (0.5 mL) and stirred at room temperature for 4 h. A superhydrophobic Ni-$CoFe_2O_4$ foam floating layer was obtained after drying at 140 °C for 1 h. The structure of the solar evaporator was the superhydrophobic floating layer, the filter paper layer and the photothermal conversion layer from bottom to top.

2.3. Characterization

The structure of Ni, $CoFe_2O_4$ and superhydrophobic $CoFe_2O_4$ was obtained by TEM (FEI Tecnai F30) and XRD (Bruker D8w). The morphology of Ni, Ni-$CoFe_2O_4$ and superhydrophobic Ni-$CoFe_2O_4$ foams was obtained by FESEM (Zeiss Company, Ltd., Munich, Germany). The surface components of the superhydrophobic Ni-$CoFe_2O_4$ foam were obtained by XPS (ESC PHI500). The surface wettability of the foam was measured by a contact angle gauge (JC2000C1). The LSV curves of the foams were obtained via an electrochemical workstation (Gamry Reference 3000). The surface temperature of the Ni-$CoFe_2O_4$ foam was measured by an infrared camera (Fluke TiS20 + MAX).

3. Results and Discussion

The flexibility and three-dimensional structure of nickel foam make it an excellent carrier. The rough surface of Ni foam was observed from its morphology (Figure 1a). The surface of the Ni foam where $CoFe_2O_4$ was grown became rougher. Importantly, on the basis of retaining the micron roughness, there was also nano roughness caused by the formation of nanosheets. Finally, micron-nano roughness was formed, which was beneficial to improving the hydrophobic performance (Figure 1b). No obvious change could be seen in the morphology of Ni-$CoFe_2O_4$ after the silane treatment (Figure 1c). The element distribution was investigated based on EDS analysis. Elements including Fe, Co and F had the same shape as the Ni foam, proving that superhydrophobic Ni-$CoFe_2O_4$ was successfully prepared (Figure 1d).

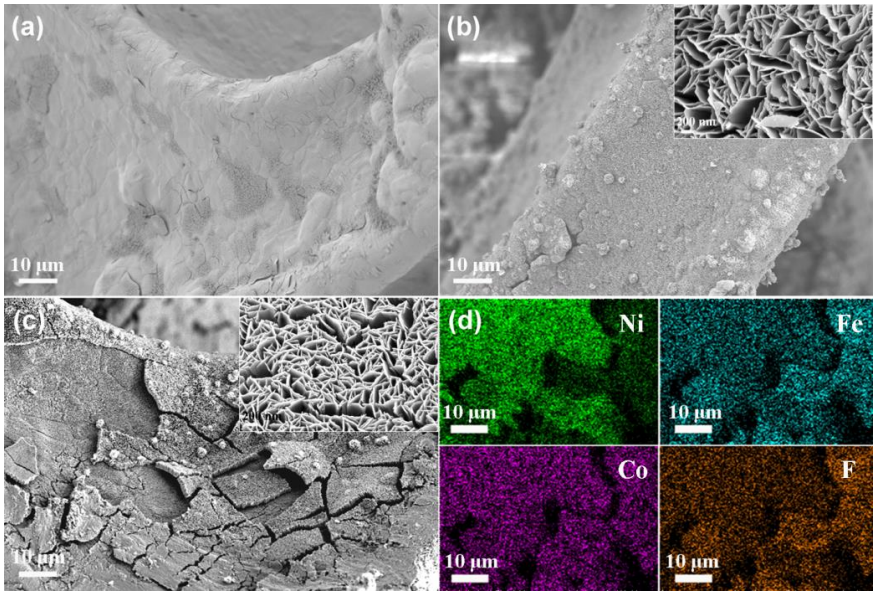

Figure 1. FESEM images of Ni foam (**a**), Ni-$CoFe_2O_4$ foam (**b**) and superhydrophobic Ni-$CoFe_2O_4$ foam (**c**). Element distribution of the superhydrophobic Ni-$CoFe_2O_4$ foam (**d**).

To analyze the surface structure and composition of the composite, the results of XRD, TEM and XPS were analyzed. Notably, the $CoFe_2O_4$ powder used in the XRD and TEM analysis was obtained through ultrasonic dissection. As shown in Figure 2a, the characteristic peaks (111), (200) and (220) of Ni found in the diffraction peaks of both $CoFe_2O_4$ and superhydrophobic $CoFe_2O_4$ indicated that Ni particles were also stripped. The characteristic peaks (200) and (220) of $CoFe_2O_4$ appeared, proving that $CoFe_2O_4$ was formed on the surface of the Ni foam, and the crystal structure of $CoFe_2O_4$ was not changed through silane grafting. The nanosheet morphology of $CoFe_2O_4$ was confirmed in the TEM image, and the lattice planes (101), (311) and (222) were analyzed based on the HRTEM image (Figure 2b). The lattice plane (111) of Ni and the lattice plane (222) as well as (440) of $CoFe_2O_4$ were analyzed based on the SAED map (Figure 2c). As shown in Figure 2d, the surface of superhydrophobic $CoFe_2O_4$ is composed of elements Co, Fe, O, Si, C and F, and the content of F is up to 48.1%, which effectively reduces the surface energy.

Further fine spectral analyses of Co and Fe revealed that $CoFe_2O_4$ had a mixed valent state consisting of Co^{2+}, Co^{3+}, Fe^{2+} and Fe^{3+} (Figure 3a,b). Relevant information of the deconvolution is presented in Table S1. The superhydrophobic Ni-$CoFe_2O_4$ foam exhibited its superhydrophobicity under the synergy of the micron-nanoscale roughness and low surface energy. As shown in Figure 3c, the water droplets spread rapidly on the surface of the Ni-$CoFe_2O_4$ foam, showing their superhydrophilicity. The inset shows that the surface exhibited a contact angle of 0° on the water. After silane treatment, the surface of the superhydrophobic Ni-$CoFe_2O_4$ foam showed a non-wetting state with a contact angle of 157°. To verify the organic solvent removal property of the superhydrophobic Ni-$CoFe_2O_4$ foam, cyclohexane was used as the target organic solvent. When the superhydrophobic Ni-$CoFe_2O_4$ foam contacted the interface between cyclohexane and the water, cyclohexane was adsorbed, leaving a blank water surface.

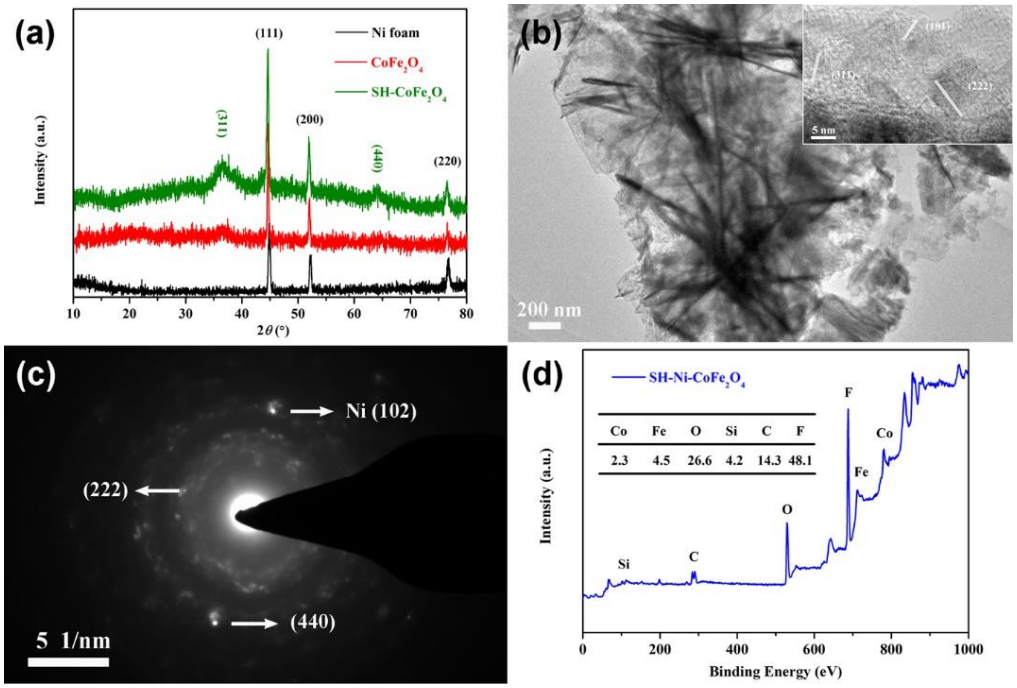

Figure 2. XRD analysis of $CoFe_2O_4$ composite materials (**a**). TEM morphology (**b**) and structure (**c**) analysis of $CoFe_2O_4$. XPS analysis (**d**) of superhydrophobic Ni-$CoFe_2O_4$.

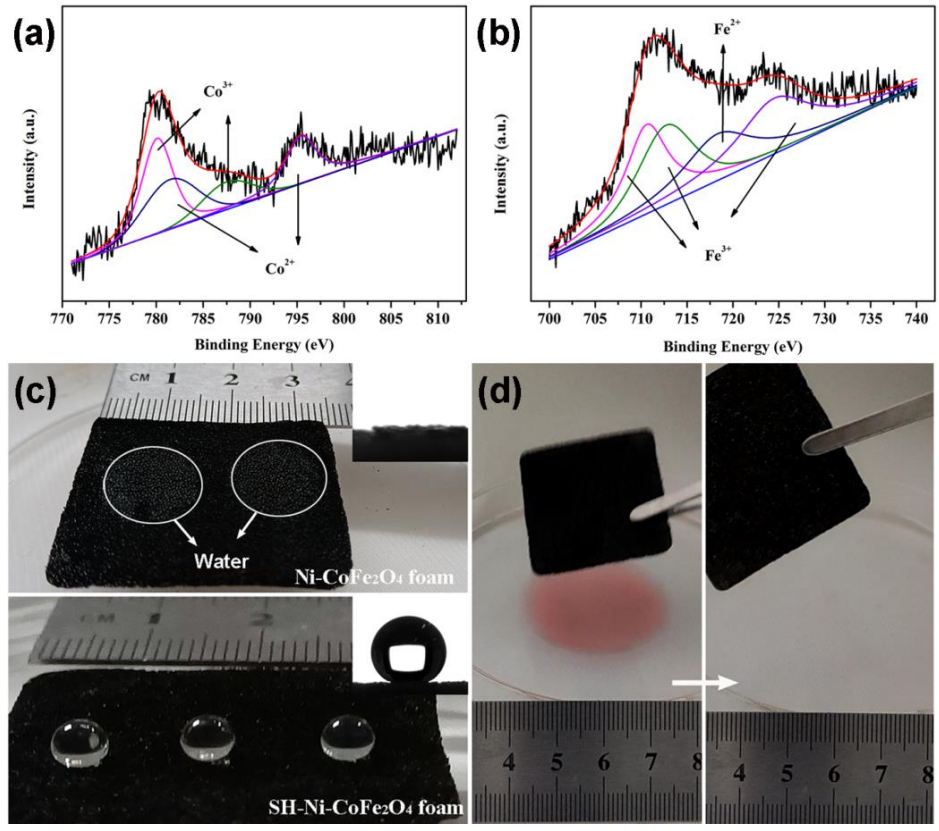

Figure 3. Fine spectrum of superhydrophobic Ni-$CoFe_2O_4$ (**a**,**b**). Image of the Ni-$CoFe_2O_4$ foam before and after silane modification (**c**). Selective organic solvent removal test for the Ni-$CoFe_2O_4$ foam (**d**).

Different from the traditional heating effect of solar energy on the whole amount of water, interface heating only works on a small amount of water, improving the efficiency of steam production. A photo of the device is shown in Figure 4a. To verify the improvement in the steam production efficiency, a comparative experiment was performed. As shown in Figure 4b, the three-layer device had the highest steam production rate (1.68 $kg \cdot m^{-2} \cdot h^{-1}$) compared with pure water, the superhydrophobic Ni-$CoFe_2O_4$ foam and the superhydrophobic Ni-$CoFe_2O_4$ foam/filter paper composite. Experiments on water drops and friction stability were designed to verify the stability of the superhydrophobic Ni-$CoFe_2O_4$ foam. The water drop was 3 cm above the surface of the superhydrophobic Ni-$CoFe_2O_4$ foam. In the friction test, the sample size was 1.5 cm × 1.5 cm, and the load was 130 g. Sandpaper served as a friction surface. After the dripping of 1000 droplets and a friction test for 200 cycles, a contact angle of greater than 150° remained on the surface of the superhydrophobic Ni-$CoFe_2O_4$ foam, demonstrating an excellent superhydrophobic stability (Figure 4c). In addition, the $CoFe_2O_4$ foam composite prepared could be used as a water oxidation electrocatalyst. A three-electrode system (the sample was taken as the working electrode, a saturated calomel electrode was used as the reference electrode and a graphite rod was used as the counter electrode) and an electrolyte of 1 M KOH were used in the LSV test. The conversion between the saturated calomel electrode (*SCE*) and the *RHE* was calculated through the following formula:

$$E(RHE) = E(SCE) + 0.059pH + 0.241 \quad (1)$$

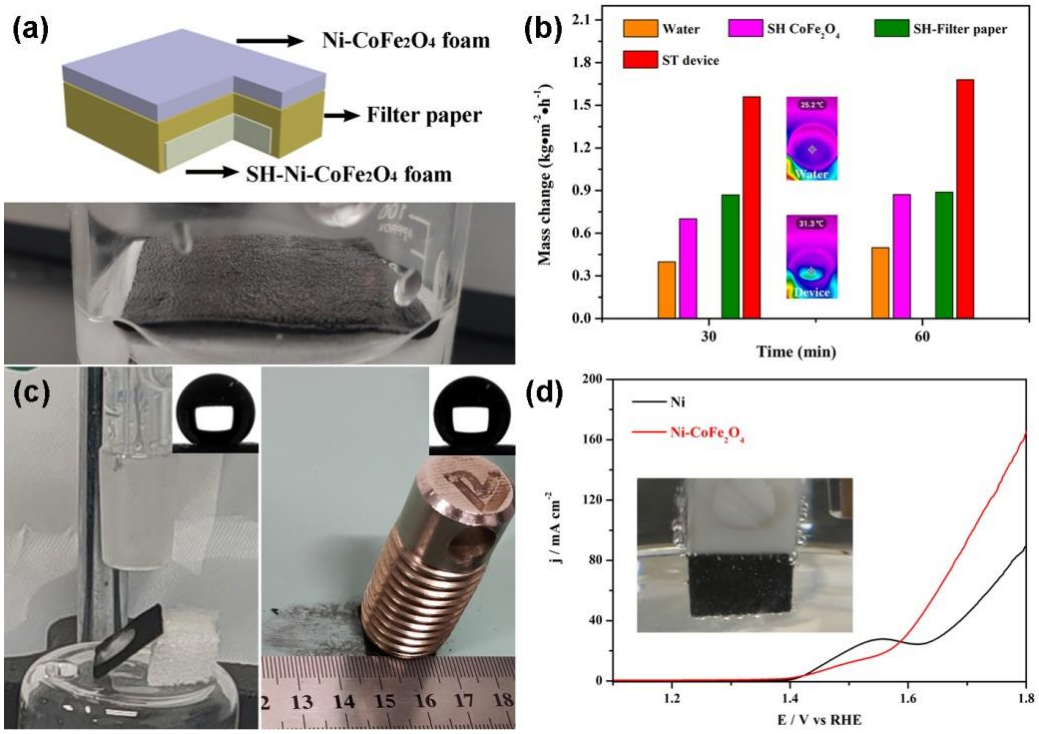

Figure 4. Schematic image of the solar steam device (**a**). Comparative experiment on the velocity of steam production (**b**). Stability test of the superhydrophobic Ni−$CoFe_2O_4$ foam (**c**). LSV curves of the $CoFe_2O_4$ composites (**d**). The inset of Figure 4b shows the surface temperature of the pure water surface and the device given by the infrared camera. Inset of Figure 4d shows the phenomenon of oxygen production in the working electrode.

Due to the 1M KOH solution used in the testing process, the pH was 14. As shown in Figure 4d, the starting potential of the Ni-$CoFe_2O_4$ foam was less than that of the Ni foam, and the phenomenon of oxygen production was observed in the working electrode.

Through device design, not only the removal of the floating organic solvent and clean water production, but also the multifunctionality of the device was realized.

4. Conclusions

In this paper, $CoFe_2O_4$ was grown on Ni foam through hydrothermal synthesis, and a superhydrophobic Ni-$CoFe_2O_4$ foam was prepared through silane modification. $CoFe_2O_4$ had a scaly morphology, and the crystal structure of $CoFe_2O_4$ was not changed after the hydrophobic modification. $CoFe_2O_4$ was proved to be the mixture valence state of Co^{2+}, Co^{3+}, Fe^{2+} and Fe^{3+}. The contact angle of the superhydrophobic Ni-$CoFe_2O_4$ foam reached 157°, which had an excellent selective organic solvent removal property. The device consisting of a superhydrophobic Ni-$CoFe_2O_4$ floating layer, a hydrophilic layer and a photothermal layer could reach a steam generation rate of 1.68 $kg{\cdot}m^{-2}{\cdot}h^{-1}$. The hydrophobic stability of the superhydrophobic Ni-$CoFe_2O_4$ foam was demonstrated through water dropping and friction experiments.

Supplementary Materials: The following are available online at https://www.mdpi.com/article/10.3390/nano12091531/s1, Table S1: Relevant information of the XPS spectrum.

Author Contributions: Writing, X.G.; Software, Z.Z.; Validation, Z.T.; Investigation, S.W.; Conceptualization, X.Z.; Methodology, G.R.; Supervision, B.G.; Reviewing and Editing, W.L. All authors have read and agreed to the published version of the manuscript.

Funding: This research was funded by the Natural Science Foundation of Shandong Province grant number ZR2021ME083 and the Innovation Team of Higher Educational Science and Technology Program in Shandong Province grant number 2019KJA025.

Data Availability Statement: The data used to support the findings of this study are included within the article.

Acknowledgments: The authors acknowledge the Natural Science Foundation of Shandong Province (Grant No. ZR2021ME083) and the Innovation Team of Higher Educational Science and Technology Program in Shandong Province (No. 2019KJA025).

Conflicts of Interest: The authors declare no conflict of interest.

References

1. Jia, Y.; Liu, P.B.; Wang, Q.Y.; Wu, Y.; Cao, D.D.; Qiao, Q.A. Construction of Bi_2S_3-BiOBr nanosheets on TiO_2 NTA as the effective photocatalysts: Pollutant removal, photoelectric conversion and hydrogen generation. *J. Colloid Interf. Sci.* **2021**, *585*, 459–469. [CrossRef] [PubMed]
2. Li, Y.S.; Wu, T.; Shen, H.; Yang, S.W.; Qin, Y.; Zhu, Z.M.; Zheng, L.; Wen, X.J.; Xia, M.G.; Yin, X.Z. Flexible MXene-based Janus porous fibrous membranes for sustainable solar-driven desalination and emulsions separation. *J. Clean. Prod.* **2022**, *347*, 131324. [CrossRef]
3. Shahzad, M.W.; Burhan, M.; Ang, L.; Ng, K.C. Energy-water-environment nexus underpinning future desalination sustainability. *Desalination* **2017**, *413*, 52. [CrossRef]
4. Shahzad, M.W.; Burhan, M.; Ng, K.C. Pushing desalination recovery to the maximum limit: Membrane and thermal processes integration. *Desalination* **2017**, *416*, 54. [CrossRef]
5. Lu, X.L.; Eliemlech, M. Fabrication of desalination membranes by interfacial polymerization: History, current efforts, and future directions. *Chem. Soc. Rev.* **2021**, *50*, 6290. [CrossRef] [PubMed]
6. Cheng, S.N.; Li, Y.H.; Jin, B.C.; Yu, Z.; Gu, R.N. Designing salt transmission channel of solar-driven multistage desalination device for efficient and stable freshwater production from seawater. *Desalination* **2022**, *531*, 115688. [CrossRef]
7. Zheng, Z.H.; Liu, H.; Wu, D.Z.; Wang, X.D. Polyimide/MXene hybrid aerogel-based phase-change composites for solar-driven seawater desalination. *Chem. Eng. J.* **2022**, *440*, 135862. [CrossRef]
8. Chen, Y.; Yang, J.; Zhu, L.; Jia, X.H.; Wang, S.Z.; Li, Y.; Song, H.J. An integrated highly hydrated cellulose network with a synergistic photothermal effect for efficient solar-driven water evaporation and salt resistance. *J. Mater. Chem. A* **2021**, *9*, 15482–15492. [CrossRef]
9. Lin, Z.X.; Wu, T.T.; Feng, Y.F.; Shi, J.; Zhou, B.; Zhu, C.H.; Wang, Y.Y.; Liang, R.L.; Mizuno, M. Poly(N-phenylglycine)/MoS_2 nanohybrid with synergistic solar-thermal conversion for efficient water purification and thermoelectric power generation. *ACS Appl. Mater. Interfaces* **2022**, *14*, 1034–1044. [CrossRef] [PubMed]

10. Wang, F.; Ma, R.R.; Zhan, J.L.; Shi, W.S.; Zhu, Y.Y.; Tian, Y.Q. Superhydrophobic/superoleophilic starch-based cryogels coated by silylated porous starch/Fe_3O_4 hybrid micro/nanoparticles for removing discrete oil patches from water. *Sep. Purif. Technol.* **2022**, *291*, 120872. [CrossRef]
11. Miao, X.; Liu, S.; Wang, M.; Ge, B.; Zhu, C.Q. Fabrication of interface heating composite evaporator for rapid sewage treatment and water purification. *Sci. China Technol. Sci.* **2021**, *64*, 2292–2299. [CrossRef]
12. Liu, Y.D.; Liu, J.H.; Wang, Z.B.; Yuan, Y.K.; Hua, J.; Liu, K. Robust and durable superhydrophobic and oil-absorbent silica particles with ultrahigh separation efficiency and recyclability. *Micropor. Mesopor. Mat.* **2022**, *335*, 111772. [CrossRef]